# Analytical Model of a Semiconductor Optical Amplifier

Philippe Brosson

*Abstract*— **The spatial dependence of the material gain is introduced in the model of a semiconductor optical amplifier. Analytical expressions of the profiles of the carrier density, spontaneous emission, and amplified fields are obtained for amplifiers with arbitrary facet reflectivities. The nonuniformity of the carrier density is demonstrated in the case of low facet reflectivities. The model predicts the output saturation power and gain ripple, with good agreement with experimental results in resonant and traveling-wave amplifiers. Very low-gain ripple measured in low facet reflectivities amplifiers is explained by the model. A comparison with the uniform gain model shows that important deviations can occur in the case of low facet reflectivities. It is also shown that with the currently achievable low facet reflectivities, the maximum available gain is limited by spontaneous emission.**

## I. Introduction

In a semiconductor optical amplifier or laser, it is usual to assume a uniform carrier distribution along the cavity length ($z$ direction) and consequently to neglect the variation of material gain with $z$. This approximation allows a very simple description of the evolution with time of carriers and photons with rate equations independent of $z$.

Lau [1] has demonstrated that in the case of lasers this approximation is no more justified for intensity reflectivities lower than 0.2. This spatial dependence has been investigated theoretically in lasers with low facet reflectivities [2], [3].

High-gain and low-ripple semiconductor amplifiers are now currently achievable [4] by using reflectivities in the range $10^{-4}$ to $10^{-5}$. In these structures, the carrier density and gain are highly nonuniform and the usual rate equations are no more acceptable.

Very few publications on semiconductor optical amplifiers take into account this spatial dependence. Numerical methods are required to obtain the static [5] or dynamic [6] solution of the $z$ dependent rate equations.

We propose an analytical model of a semiconductor optical amplifier, taking into account this spatial dependence [7]. The model gives analytical expressions for the carrier density, spontaneous emission, and amplified field profiles and can predict gain saturation effects and gain ripple in traveling-wave or resonant amplifiers.

Manuscript received April 16, 1993; revised July 6, 1993. This work was supported in part by EEC RACE 2039 ATMOS program.

The author is with Alcatel Alsthom Recherche, Marcoussis, France.

IEEE Log Number 9213468.

## II. Model

We start from the model of Adams *et al.* [8] and introduce the spatial dependence of the carriers and photons. The laser amplifier is described by a set of rate equations involving forward- and backward-propagating spontaneous photon densities and amplified field amplitudes, and carrier density, including $z$ dependence.

$$\frac{\partial X^+}{\partial t} + c\frac{\partial X^+}{\partial z} = c[\Gamma a(N - N_t) - \alpha]X^+ + \Gamma\frac{\beta}{2}\frac{N}{\tau} \quad (1)$$

$$\frac{\partial X^-}{\partial t} - c\frac{\partial X^-}{\partial z} = c[\Gamma a(N - N_t) - \alpha]X^- + \Gamma\frac{\beta}{2}\frac{N}{\tau} \quad (2)$$

$$\frac{\partial F^+}{\partial t} + c\frac{\partial F^+}{\partial z} = \frac{1}{2}c[\Gamma a(N - N_t) - \alpha]F^+ - ik_s cF^+ \quad (3)$$

$$\frac{\partial F^-}{\partial t} - c\frac{\partial F^-}{\partial z} = \frac{1}{2}c[\Gamma a(N - N_t) - \alpha]F^- - ik_s cF^- \quad (4)$$

$$\frac{\partial N(z,t)}{\partial t} = \frac{J}{qd} - \frac{N}{\tau} - ca(N - N_t)[X^+ + X^- + |F^+|^2 + |F^-|^2] \quad (5)$$

The symbols used are summarized in Table I

| Symbol | Definition | units |
|---|---|---|
| $X^{\pm}(z)$ | propagating amplified spontaneous photon density, forward and backward | $m^{-3}$ |
| $x^{\pm}(z)$ | normalized $X^{\pm}(z)$, $x^{\pm}(z) = ca\tau X^{\pm}(z)$ | |
| $F^{\pm}(z)$ | amplified field amplitude, forward and backward | $m^{-3/2}$ |
| $y^{\pm}(z)$ | normalized $F^{\pm}(z)$, $y^{\pm}(z) = (ca\tau)^{1/2}F^{\pm}(z)$ | |
| $y_{\text{refl}}$ | normalized reflected signal field | |
| $y_{\text{out}}$ | normalized outgoing signal field | |
| $y_{\text{in}}$ | normalized incident signal field, $y_{\text{in}} = (a\tau\Gamma P_{\text{in}}/wdh\nu_s)^{1/2}$ | |
| $P_{\text{in}}, P_{\text{sat}}$ | incident optical power, output saturation power | mW |
| $n_{\text{eff}}$ | effective index | |
| $\lambda_s$ | wavelength of the incident signal | m |
| $k_s$ | wave vector of the incident signal $k_s = 2\pi$ neff $/\lambda_s$ | $m^{-1}$ |
| $h\nu_s$ | photon energy of the incident signal | J |
| $k_r$ | wave vector of the resonant Fabry-Perot modes | $m^{-1}$ |
| $\lambda_r, \lambda_{ar}$ | wavelength of the resonant and anti-resonant Fabry-Perot modes | m |
| $t$ | time | s |
| $z$ | cavity length direction, $z = 0$ is the center of the amplifier | m |
| $c$ | group velocity | $m\ s^{-1}$ |
| $\Gamma$ | transverse optical confinement factor | |
| $a$ | linear material gain coefficient | $m^2$ |
| $N(z)$ | carrier density profile | $m^{-3}$ |
| $n(z)$ | normalized carrier density profile, $n(z) = N(z)/(J\tau/qd)$ | |
| $N_t$ | carrier density at transparency | $m^{-3}$ |

| | | |
|---|---|---|
| $\alpha$ | modal optical loss (intensity) | $m^{-1}$ |
| $\beta$ | spontaneous emission factor | |
| $\tau$ | carrier lifetime | s |
| $J$ | injected current density | A $m^{-2}$ |
| $q$ | electronic charge | C |
| $d, L, w$ | thickness, length, width of the amplifier | m |
| $R_1, R_2$ | input, output intensity facet reflectivities | |
| $u(z)$ | real function entering in the carrier density, spontaneous emission and amplified field profiles | |
| $a_1, a_2$ | real coefficients for $x^{\pm}(z)$ | |
| $b_1, b_2$ | complex coefficients for $y^{\pm}(z)$ | |
| $e, f$ | $e = \exp[\Gamma u(L/2)], f = \exp[-\Gamma u(-L/2)]$ | |
| $G(\lambda_s)$ | gain of the amplifier | |
| $G_{\text{unif}}(\lambda_s), Gs$ | gain of the amplifier, single-pass gain (uniform gain model) | |

The amplified spontaneous emission is treated incoherently [8] by forward and backward photon densities $X^{\pm}$. In (1) and (2), the factor 1/2 accounts for positive and negative propagation. The propagating signal is represented by forward and backward amplitude fields.

We have made simplifying assumptions in writing (1)–(5).

1/ The gain is homogeneously broadened. This has been confirmed experimentally [9].

2/ The material gain is linear with the carrier density and constant with photon energy in the wavelength range of interest (close to the peak gain).

3/ The transverse effects are described by the optical confinement factor $\Gamma$.

4/ Carrier diffusion is ignored.

5/ The recombination rate is described by a constant carrier lifetime. An effective carrier lifetime $\tau$ can be used to include nonradiative recombination such as Auger. Using the values [10] of the radiative and nonradiative recombination coefficients, the carrier lifetime lies between 3 and 1 ns and the differential carrier lifetime between 1.7 and 0.5 ns, for carrier densities ranging from 2 to $5 \times 10^{18} \text{cm}^{-3}$. The static behavior will be obtained by using for $\tau$ the total carrier lifetime (2 ns) and by injecting the carrier density in (1)–(4), leading to a set of four differential equations in $z$.

6/ Polarization is not analysed. $TE$ and $TM$ gains could be obtained with $TE$ and $TM$ reflectivities and optical confinement factors.

In the following, we have assumed $\alpha = 0$ and $N_t = 0$ for technical simplicity, but not for fundamental reasons.

By setting time derivatives to zero, we obtain

$$dx^+/dz = +\Gamma a N(x^+ + \beta/2) \tag{6}$$

$$dx^-/dz = -\Gamma a N(x^- + \beta/2) \tag{7}$$

$$dy^+/dz = +(1/2)\Gamma a N y^+ - ik_s y^+ \tag{8}$$

$$dy^-/dz = -(1/2)\Gamma a N y^- + ik_s y^- \tag{9}$$

$$N(z) = \frac{J\tau/qd}{1 + x^+(z) + x^-(z)|y^+(z)|^2 + |y^-(z)|^2} \tag{10}$$

where we have normalized $X^{\pm}$ and $F^{\pm}$ by $x^{\pm}(z) = ca\tau X^{\pm}(z), y^{\pm}(z) = (ca\tau)^{1/2} F^{\pm}(z)$ By substitution of (10) into (6) and( 7) we obtain

$$\frac{d(x^+ + \beta)/dz}{x^+ + \beta} = \Gamma \frac{(aJ\tau)/(qd)}{1 + x^+(z) + x^-(z) + |y^+(z)|^2 + |y^-(z)|^2} \tag{11}$$

$$\frac{d(x^- + \beta)/dz}{x^- + \beta} = -\Gamma \frac{(aJ\tau)/(qd)}{1 + x^+(z) + x^-(z) + |y^+(z)|^2 + |y^-(z)|^2} \tag{12}$$

$$\frac{dy^+/dz}{y^+} = \frac{\Gamma}{2} \frac{(aJ\tau)/(qd)}{1 + x^+(z) + x^-(z) + |y^+(z)|^2 + |y^-(z)|^2} - ik_s \tag{13}$$

$$\frac{dy^-/dz}{y^-} = \frac{-\Gamma}{2} \frac{(aJ\tau)/(qd)}{1 + x^+(z) + x^-(z) + |y^+(z)|^2 + |y^-(z)|^2} + ik_s \tag{14}$$

It is straightforward to verify that (11)–(14) have the solutions

$$x^+(z) = a_1 \exp[\Gamma u(z)] - \beta/2 \tag{15}$$

$$x^-(z) = a_2 \exp[-\Gamma u(z)] - \beta/2 \tag{16}$$

$$y^+(z) = b_1 \exp[(1/2)\Gamma u(z)] \exp[-ik_s z] \tag{17}$$

$$y^-(z) = b_2 \exp[-(1/2)\Gamma u(z)] \exp[ik_s z] \tag{18}$$

and that the real function $u(z)$ must satisfy the differential equation

$$\frac{du}{dz} = \frac{(aJ\tau)/(qd)}{1 + x^+(z) + x^-(z) + |y^+(z)|^2 + |y^-(z)|^2} \tag{19}$$

and that $N(z)$ is obtained by substitution of (15)–(18) into (10)

$$N(z) = J\tau/qd \Big/ 1 - \beta + [a_1 + |b_1|^2] \text{ Exp } [\Gamma u(z)] + [a_2 + |b_2|^2] \text{ Exp } [-\Gamma u(z)] \tag{20}$$

Substituting (15)–(18) into (19) gives $du/dz$

$$\frac{du}{dz} = aJ\tau/qd \Big/ 1 - \beta + [a_1 + |b_1|^2]\text{Exp}[\Gamma \text{u(z)}] + [a_2 + |b_2|^2]\text{Exp}[-\Gamma u(z)] \tag{21}$$

The transcendental equation for $u(z)$ is obtained by integrating the differential (21).

$$\Gamma(1 - \beta)u + [a_1 + |b_1|^2] \exp(\Gamma u) - [a_2 + |b_2|^2] \exp(-\Gamma u) = \Gamma(aJ\tau/qd)z \tag{22}$$

The real $a_1, a_2$, and complex $b_1, b_2$ constants are determined by the boundary conditions on the facets at $z = \pm L/2$ (Fig. 1).

$$x^+(-L/2) = R_1 x^-(-L/2) \tag{23}$$

$$x^-(+L/2) = R_2 x^+(+L/2) \tag{24}$$

$$y^+(-L/2, \lambda_s) = (1 - R_1)^{1/2} y_{\text{in}} + \sqrt{R_1} y^-(-L/2, \lambda_s) \tag{25}$$

$$y^-(+L/2, \lambda_s) = \sqrt{R_2} y^+(+L/2, \lambda_s) \tag{26}$$

$$y_{\text{refl}} = (1 - R_1)^{1/2} y^-(-L/2, \lambda_s) \tag{27}$$

$$y_{\text{out}} = (1 - R_2)^{1/2} y^+(+L/2, \lambda_s) \tag{28}$$

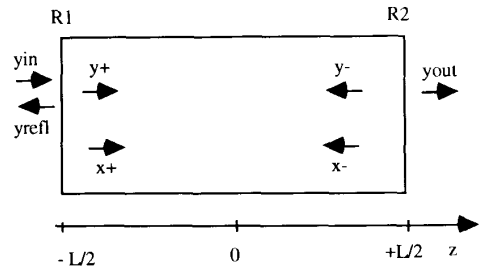


Fig. 1. Schematic of optical amplifier showing the normalized field amplitudes $y_{in}, y_{out}, y^+, y^-$ and the spontaneous photon density $x^+, x^-$.

Solving (23)–(28) leads to explicit expressions for the coefficients $a_1$, $a_2$, $|b_1|^2$ and $|b_2|^2$

$$a_1 = \frac{\beta}{2}\frac{1 - R_1 + (1 - R_2)R_1 ef}{1 - R_1 R_2 (ef)^2} f \tag{29}$$

$$a_2 = \frac{\beta}{2}\frac{1 - R_2 + (1 - R_1)R_2 ef}{1 - R_1 R_2 (ef)^2} e \tag{30}$$

$$|b_1|^2 = \frac{(1 - R_1) y_{\text{in}}^2 f}{[1 - \sqrt{R_1 R_2}ef]^2 + 4\sqrt{R_1 R_2}ef \sin^2[(k_s - k_r)L]} \tag{31}$$

$$|b_2|^2 = \frac{(1 - R_1) R_2 y_{\text{in}}^2 f e^2}{[1 - \sqrt{R_1 R_2}ef]^2 + 4\sqrt{R_1 R_2}ef \sin^2[(k_s - k_r)L]} \tag{32}$$

In (29)–(32) we have defined $e = \exp[\Gamma u(L/2)]$ and $f = \exp[-\Gamma u(-L/2)]$. By using (29)–(32) and (22) for $z = \pm L/2$, we obtain a set of two equations in $e$ and $f$ that can be solved numerically. With the knowledge of $a_1, a_2, |b_1|^2$, and $|b_2|^2$, the functions $u(z), x^{\pm}(z)$, and $y^{\pm}(z)$ are therefore completely determined and the carrier density profile is given by (20).

The incident power $P_{\text{in}}$ is related to the normalized incident field $y_{\text{in}}$ by

$$y_{\text{in}} = (a\tau\Gamma P_{\text{in}}/wdh\nu_s)^{1/2} \tag{33}$$

and the gain $G(\lambda_s) = |y_{\text{out}}|^2/y_{\text{in}}^2$ is given by

$$G(\lambda_s) = \frac{(1 - R_1)(1 - R_2)ef}{[1 - \sqrt{R_1 R_2}ef]^2 + 4\sqrt{R_1 R_2}ef \sin^2[(k_s - k_r)L]} \tag{34}$$

where the $k_r$ are the wave vectors of the resonant modes of the Fabry-Perot amplifier. The incident power is implicitly included in (34) through $e$ and $f$ since $e$ and $f$ depend on $y_{in}$. Therefore (34) gives the saturated gain.

In the special case of a uniform carrier density profile $N(z) = N, u(z) = aNz$, (34) reduces to the well-known result of an active Fabry-Perot amplifier and saturation is not taken into account

$$G_{\text{unif}}(\lambda_s) = \frac{(1 - R_1)(1 - R_2)G_s}{[1 - \sqrt{R_1 R_2}Gs]^2 + 4\sqrt{R_1 R_2}Gs \sin^2[(k_s - k_r)L]} \tag{35}$$

where $Gs = \exp[\Gamma aNL]$ is the single-pass gain.

The gain is maximum at the resonant modes ($k_s = k_r$) and minimum for ( $k_s - k_r)L = \pi/2$. The ripple gain defined as $G(\lambda_r)/G(\lambda_{\text{ar}})$ is derived from Eq. (34)

$$\frac{G(\lambda_r)}{G(\lambda_{\text{ar}})} = \frac{e(\lambda_r)f(\lambda_r)}{e(\lambda_{\text{ar}})f(\lambda_{\text{ar}})} \frac{[1 + \sqrt{R_1 R_2}e(\lambda_{\text{ar}})f(\lambda_{\text{ar}})]^2}{[1 - \sqrt{R_1 R_2}e(\lambda_r)f(\lambda_r)]^2} \tag{36}$$

In the case of a uniform carrier density profile, (36) reduces to

$$\frac{G_{\text{unif}}(\lambda_r)}{G_{\text{unif}}(\lambda_{\text{ar}})} = \frac{[1 + \sqrt{R_1 R_2}G_s]^2}{[1 - \sqrt{R_1 R_2}G_s]^2} \tag{37}$$

In the following, the current density $J$ is normalized by the threshold current density

$$J_{\text{th}} = \frac{qd}{\tau}\left[N_t + \frac{1}{\Gamma a}\left(\frac{1}{L}Ln\left[\frac{1}{\sqrt{R_1 R_2}}\right] + \alpha\right)\right] \tag{38}$$

These analytical expressions have been programmed in Mathematica [11] language, leading to computing times of only a few minutes on a Sun SPARC 10 workstation. In all calculations we have used $n_{\text{eff}} = 3.5$, $\lambda = 1.55\mu$m, $\Gamma = 0.4$, $a = 2.5 \times 10^{-16}$ cm$^2$, $\tau = 2$ ns, $d = 0.2\mu$m, $L = 300\mu$m, and $w = 2\mu$m.

## III. Profiles of the Carrier Density, Spontaneous Photon Density and Amplified Signal Fields

Fig. 2 shows the profiles of the carrier density $n(z)$, the total spontaneous photon density $x^+(z) + x^-(z)$, and the amplified signal fields $s^+(z) = |y^+(z)|^2, s^-(z) = |y^-(z)|^2$, in the case of resonant amplifier ($R_1 = R_2 = 0.3$) and traveling-wave amplifier ($R_1 = R_2 = 10^{-4}$). For these calculations, we have used $\beta = 10^{-3}$, a normalized pumping rate $J/J_{\text{th}} = 0.9$ and an incident signal tuned on a Fabry-Perot resonance. Two values of the input power are considered: $-40$ dBm (unsaturated gain) and $-10$ dBm (saturated gain) to illustrate the longitudinal gain saturation.

In the first case, $n(z)$ is almost uniform, even at high input power. On the other hand, $n(z)$ is strongly reduced near the facet where the amplified spontaneous emission or signal is high, as described by (10).

At low input power, $n(z)$ is mainly determined by the spontaneous emission and is consequently symmetrical since $R_1 = R_2$.

The evolution of these profiles with the incident signal level clearly shows that $n(z)$ reduces asymmetrically at high input power, with a maximum near the input facet. These results demonstrate that the uniform carrier distribution approximation is justified only in the case of the resonant amplifier.

We have also calculated these profiles for $R_1 \neq R_2$ and obtained a nonuniform carrier distribution if one of the facets has a low reflectivity. For the investigated value $\beta = 10^{-3}$, low reflectivity means lower than 0.1–0.2.

## IV. Gain Saturation Effects and Gain Ripple

In Figs. 3 and 4, we compare our results with those of Buus, Fig. 1 [12] in the case of a resonant amplifier and those of Marcuse, Fig. 7 [5] in the case of a traveling-wave amplifier.

In Fig. 3 we have calculated the gain as a function of current, for $\beta = 10^{-4}$ and input power $P_{\text{in}} = -40$ and $-30$ dBm, using the parameters of [12], with the exception of internal losses and carrier density at transparency. Since in the case of cleaved facets the carrier distribution is almost uniform, a good agreement is expected with the model of Buus [12], which neglects this nonuniformity. The higher gain that we

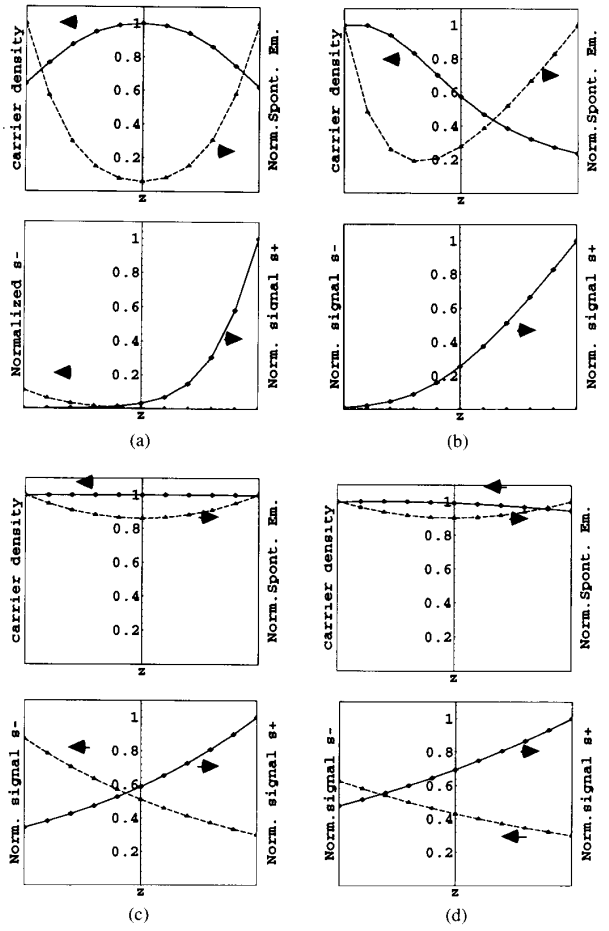


Fig. 2. Profiles of the carrier density $n(z)$, the total spontaneous photon density $x^+(z) + x^-(z)$, and the amplified signal fields $s^+(z) = 1y^+(z)1^2, s^-(z) = 1y^-(z)1^2$ for $\lambda_r = \lambda_r, \beta = 1 \times 10^3, J/J_{th} = 0.9$. (a)$R_1 = R_2 = 10^{-4}.P_{in} = -40$ dBm. (b) $R_1 = R_2 = 10^{-4}.P_{in} = -10$ dBm. (c) $R_1 = R_2 = 0.3.P_{in} = -40$dBm. (d) $R_1 = R_2 = 0.3.P_{in} = -10$ dBm.

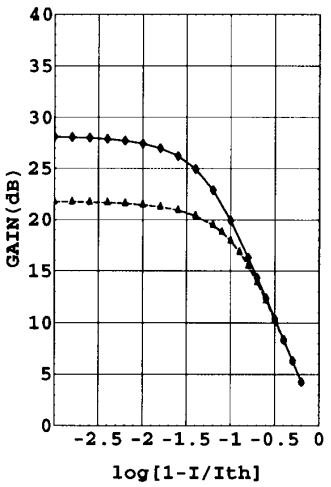


Fig. 3. Gain as a function of current, in a resonant amplifier, for $\beta = 10^{-4}$, calculated using the parameters of [12], but with $\alpha = 0$ and $N_t = 0$. From top to bottom, $P_{in} = -40$dBm to $-30$dBm.

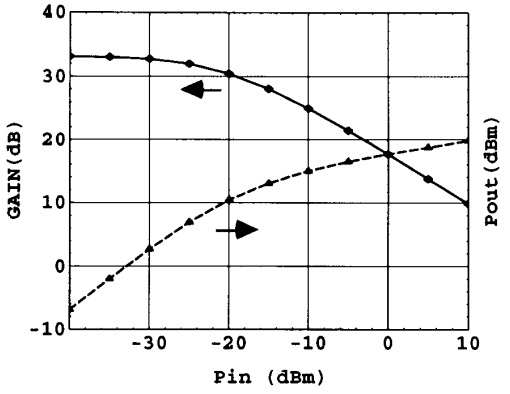


Fig. 4. Gain and output power as a function of input power, in a traveling-wave amplifier, calculated using the parameters of [5], but with $\alpha = 0$ and $N_t = 0$. The saturation input power is —19.4 dBm.

have obtained is due to the fact that we have used $\alpha = 0$ and $N_t = 0$.

In [12], it is shown that in the case of low input power, and $I/I_{\text{th}} \ll 1, G = G^*(1 - I/I_{\text{th}})^{-2}$, with $G^* = \frac{(1-R_1)(1-R_2)}{\left(\alpha L + Ln\frac{1}{\sqrt{R_1R_2}} + \Gamma a N_t L\right)^2 \sqrt{R_1R_2}}$, giving $G^* = -13.5$ dB.

For $I/I_{\text{th}} \ll 1$, we obtain a slope of $-2$, indicating a decrease of the gain proportional to $(1 - I/I_{\text{th}})^{-2}$, in agreement with [12].

With $\alpha = 0$ and $N_t = 0$, we obtain $G^* = 0.45$ dB and in the linear part of the gain curve (Fig. 3), the correction would be 13.95 dB, which is in agreement with Fig. 1 of [12]

In Fig. 4 we show the gain and the output power as a function of input power, in a traveling-wave amplifier, calculated using the parameters of [5], except for $\alpha$ and $N_t$. When the input power increases from $-40$ dBm to 10 dBm, we calculate that the gain decreases from 33 to 9.8 dB. This decrease is comparable to the values (30 to 4 dB) reported by [5]. The difference is attributed to our approximation on $\alpha$ and $N_t$. On Fig. 4, the saturation input power is $-19.4$ dBm, which is in good agreement with the value of $-20$ dBm that can be read in Fig. 7 of [5].

The amplifier gain has been calculated under the same conditions as in Section III, using (34). Fig. 5 presents the gain as a function of output power for $R_1 = R_2 = 10^{-4}$ with $\beta = 10^{-4}, 10^{-3}$ and $4 \times 10^{-3}$ and also for $R_1 = R_2 = 0.3$ with $\beta = 10^{-3}$. At high input power, the gain is mainly reduced by the signal. At low input power, the gain is reduced by the loss of carriers due to the spontaneous emission recombination. The value of $\beta$ affects the so-called linear gain. The gain decreases if $\beta$ increases, as pointed out by [12], due to a stronger reduction of the carrier density.

The output saturation power is defined as the output power at which the gain is reduced by 3 dB. In the case $\beta = 4 \times 10^{-3}$, $P_{\text{sat}} = 6$ dBm for the traveling-wave amplifier (Fig. 5). The

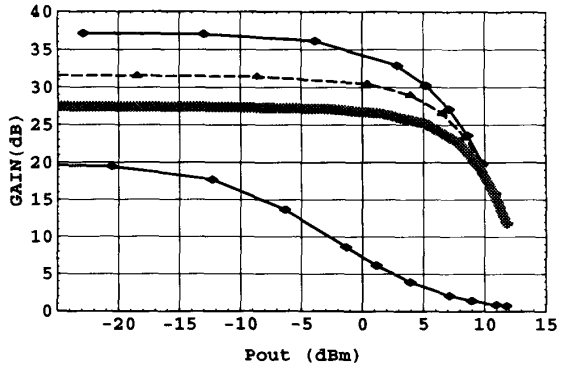


Fig. 5. Maximum gain as a function of output power for different values of the spontaneous emission coefficient $\beta$ and facet reflectiveness $R_1, R_2. J/J_{th} = 0.9$. From top to bottom: $\beta = 1 \times 10^4, R_1 = R_2 = 10^{-4}, P_{sat} = 1$dBm; $\beta = 1 \times 10^{-3}, R_1 = R_2 = 10^{-4}, P_{sat} = 4.6$dBm; $\beta = 4 \times 10^{-3}, R_1 = R_2 = 10^{-4}$, $P_{sat} = 6$dBm; and $\beta = 1 \times 10^{-3}, R_1 = R_2 = 0.3, P_{sat} = -11$dBm.

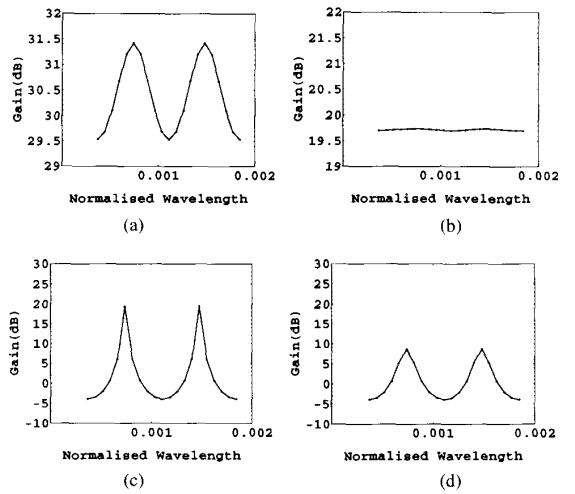


Fig. 6. Gain as a function of incident signal wavelength. $J/J_{th} = 0.9$.(a) $R_1 = R_2 = 10^-4, P_{in} = -40$dBm. (b) $R_1 = R_2 = 10^-4, P_{in} = -10$dBm. (c) $R_1 = R_2 = 0.3, P_{in} = -40$dBm. (d) $R_1 = R_2 = 0.3, P_{in} = -10$dBm.

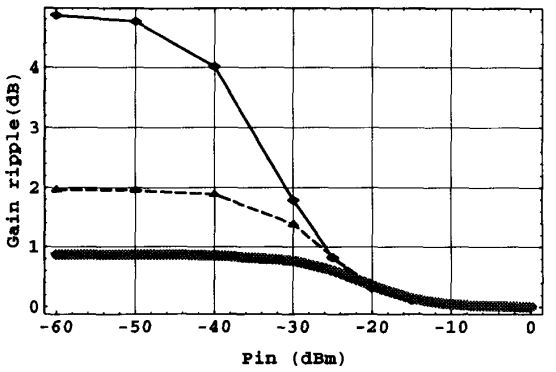


Fig. 7. Gain ripple as a function of incident signal power for $R_1 = R_2 = 10^{-4}, J/J_{th} = 0.9$. From top to bottom: $\beta = 1 \times 10^{-4}, \beta = 1 \times 10^{-3}, \beta = 1 \times 10^{-3}$.

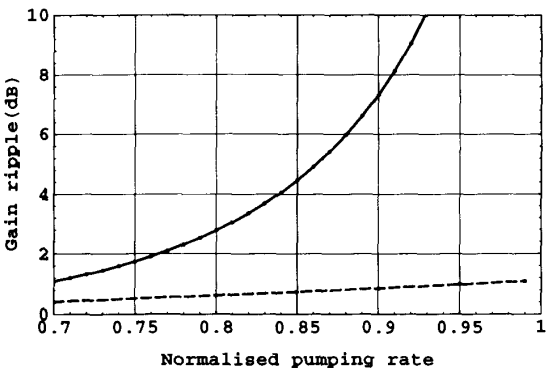


Fig. 8. Calcualted gain ripple for $R_1 = R_2 = 10^{-4}, \beta = 4 \times 10^{-3}$ and $P_{in} = -40$dBm as a function of normalized pumping rate $J/J_{th}$. Top curve uses (37), uniform gain model; bottom curves uses (36), this model.

experimental values of $P_{\text{sat}}$ lie between 5 and 15 dBm, this spread in $P_{\text{sat}}$ values being attributed mainly to $\beta$, which depends on the geometry and inversion level of the amplifier.

For a given value of $\beta$, $P_{\text{sat}}$ and the gain are higher in the traveling-wave amplifier. This behavior is in agreement with experimental results.

With this model, the effect of saturation on the gain ripple can be obtained from (34) and compared to the uniform gain model. Fig. 6 shows the gain as a function of signal wavelength under the same conditions as in Fig. 2. In the case $R_1 = R_2 = 10^{-4}$, the gain ripple is 2 dB and 0.04 dB, respectively, at $-40$ dBm and $-10$ dBm. This very low gain ripple is due to gain saturation. With the uniform gain model, a 7-dB gain ripple would be obtained with (37), whatever the value of $P_{\text{in}}$ or $\beta$.

In the case $R_1 = R_2 = 0.3$, the gain ripple is 24 dB and 13 dB, respectively, at $-40$ dBm and $-10$ dBm. This important gain ripple is due to the high reflectivity. With the uniform gain model, a 24-dB gain ripple would be obtained.

Fig. 7 summarized the gain ripple calculated for $\beta = 1 \times 10^{-4}$, $1 \times 10^{-3}$, $4 \times 10^{-3}$, in the case $R_1 = R_2 = 10^{-4}$.

Gain saturation has the advantage of reducing the gain ripple. Fig. 8 shows the calculated gain ripple for $R_1 = R_2 = 10^{-4}$ and $P_{\text{in}} = -40$ dBm as a function of $J/J_{th}$. For comparison, we also present the gain ripple given by (37). This equation neglects gain saturation and as $G_s$ approaches the threshold value $1/\sqrt{R_1 R_2}$, gain ripple becomes infinite. With saturation, the gain ripple remains below 1 dB (Fig. 8).

Such low gain ripple (0.8 dB) has been measured [4] and could not be explained with the uniform gain model . Even for $R_1 = R_2 = 10^{-5}$, (37) gives a 6-dB gain ripple. For $\beta = 4 \times 10^{-3}$ the calculated gain ripple with (36) is 0.8 dB (Fig. 8).

We have also calculated the gain for lower reflectivities in order to determine the maximum available gain with currently achievable facet reflectivities. By reducing the facet reflectivity from $10^{-4}$ to $10^{-5}$, the gain ($\beta = 4 \times 10^{-3}, P_{\text{in}} = -60$ dBm,

$J/J_{th} = 0.9$) is only improved from 27.4 to 29.6 dB. However, the gain ripple is reduced from 0.9 to 0.15 dB.

By increasing $J/J_{th}$ from 0.9 to 0.99 the gain increases only a few dB.

## V. Conclusion

We have presented an analytical model of an optical amplifier with arbitrary facet reflectivities. The nonuniformity of the carrier distribution is clearly demonstrated in the case of low reflectivities and contributes to important deviation from the uniform gain model.

Saturation effects are derived from the model and the predicted behavior is in good agreement with experiments. The very low gain ripple values observed in traveling-wave amplifiers are explained by the model. These results demonstrate that in the case of low reflectivities, it is necessary to take into account the spatial gain distribution. With the currently achievable low facet reflectivities, the maximum available gain is limited by spontaneous emission.

## Acknowledgment

The author wishes to thank J. Benoit and H. Bissessur for fruitful discussions.

## References

[1] K. Y. Lau, *Semiconductors and Semimetals*, vol. 22, pt. B. Orlando, FL: Academic Press, 1985, p. 72.

[2] B. J. Thedrez and C. H. Lee, "A reassessment of standard rate equations for low facet reflectivity semiconductor lasers using traveling wave rate equations," *IEEE J. Quantum Electron.*, vol. 28, pp. 2706–2713. Dec. 1992.

[3] L. W. Casperson, "Threshold characteristics of mirrorless lasers," *J. Appl. Phys.*, vol. 48, pp. 256–262, Jan. 1977.

[4] B. Fernier, P. Brosson, D. Bayart, P. Doussière, R. Beaumont, F. Leblond, P. Morin, G. Da Loura, J. Jacquet, E. Derouin, and P. Garabedian, "Fast (300 ps) polarization insensitive semiconductor optical amplifier switch with low driving current (70 mA)," in *Proc. 13th IEEE International Semiconductor Laser Conference*, Sept. 1992, pp. 130–131.

[5] D. Marcuse, "Computer model of an injection laser amplifier," *IEEE J. Quantum Electron.*, vol.19, pp. 63–73, Jan. 1983.

[6] T. Durhuus, B. Mikkelsen, and K. E. Stubkjaer, "Detailed dynamic model for semiconductor optical amplifiers and their crosstalk and intermodulation distortion," *J. Lightwave Technol.*, vol. 10, pp. 1056–1065, Aug. 1992.

[7] P. Brosson, "Modèle analytique d'un amplificateur à semi-conducteur", 13 èmes Journèes Nationales d'Optique Guidée, Marseille, pp. 70/1–70/4, May 1993.

[8] M. J. Adams, J. V. Collins, and I. D. Henning, "Analysis of semiconductor laser optical amplifiers," in *IEE Proc.*, vol. 132, pt. J, no. 1. Feb. 1985, pp. 58–63.

[9] P. Brosson, W. Rühle, N. B. Patel, and J. E. Ripper, "Optical coupling of two injection lasers: a new experimental approach to study the gain broadening mechanism," *IEEE J. Quantum Electron.*, vol. 17, pp. 714–717, May 1981.

[10] B. Fernier, P. Brosson, J. P. Jicquel, and J. Benoit, "1.5 $\mu$m laser with high external quantum efficiency and controlled emission wavelength," in *IEE Proc.*, vol. 134, pt. J, no. 1, 1987, pp. 27–34.

[11] Wolfram Research, Mathematica, Version 2.1, Champaign, Illinois, 1992.

[12] J. Buus and R. Plastow, "A theoretical and experimental investigation of Fabry-Perot semiconductor laser amplifiers," *IEEE J. Quantum Electron.*, vol. 21, pp. 614–618, June 1985.

**P. Brosson**, photograph and biography not available at the time of publication.